AGU PUBLICATIONS

JGR

Journal of Geophysical Research: Space Physics

RESEARCH ARTICLE
10.1002/2016JA023461

Special Section:
Major Results From the MAVEN Mission to Mars

Hot oxygen escape from Mars: Simple scaling with solar EUV irradiance

T. E. Cravens[1], A. Rahmati[2], Jane L. Fox[3], R. Lillis[2], S. Bougher[4], J. Luhmann[2], S. Sakai[1], J. Deighan[5], Yuni Lee[4], M. Combi[4], and B. Jakosky[5]

[1]Department of Physics and Astronomy, University of Kansas, Lawrence, Kansas, USA, [2]Space Science Lab, University of California, Berkeley, California, USA, [3]Department of Physics, Wright State University, Dayton, Ohio, USA, [4]Climate and Space Sciences and Engineering Department, University of Michigan, Ann Arbor, Michigan, USA, [5]LASP, University of Colorado Boulder, Boulder, Colorado, USA

Key Points:
- Photochemistry dominates oxygen escape from Mars
- Martian oxygen escape rate scales linearly with solar activity
- Dependence of O escape rate from Mars on elastic cross section is described

Correspondence to:
T. E. Cravens,
cravens@ku.edu

Citation:
Cravens, T. E., et al. (2016), Hot oxygen escape from Mars: Simple scaling with solar EUV irradiance, *J. Geophys. Res. Space Physics*, *121*, doi:10.1002/2016JA023461.

Received 13 SEP 2016
Accepted 1 DEC 2016
Accepted article online 9 DEC 2016

Abstract The evolution of the atmosphere of Mars and the loss of volatiles over the lifetime of the solar system is a key topic in planetary science. An important loss process for atomic species, such as oxygen, is ionospheric photochemical escape. Dissociative recombination of O_2^+ ions (the major ion species) produces fast oxygen atoms, some of which can escape from the planet. Many theoretical hot O models have been constructed over the years, although a number of uncertainties are present in these models, particularly concerning the elastic cross sections of O atoms with CO_2. Recently, the Mars Atmosphere and Volatile Evolution mission has been rapidly improving our understanding of the upper atmosphere and ionosphere of Mars and its interaction with the external environment (e.g., solar wind), allowing a new assessment of this important loss process. The purpose of the current paper is to take a simple analytical approach to the oxygen escape problem in order to (1) study the role that variations in solar radiation or solar wind fluxes could have on escape in a transparent fashion and (2) isolate the effects of uncertainties in oxygen cross sections on the derived oxygen escape rates. In agreement with several more elaborate numerical models, we find that the escape flux is directly proportional to the incident solar extreme ultraviolet irradiance and is inversely proportional to the backscatter elastic cross section. The amount of O lost due to ion transport in the topside ionosphere is found to be about 5–10% of the total.

1. Introduction

A key process for loss of atomic oxygen from the atmosphere of Mars is photochemical escape. Photochemistry in the upper atmosphere and ionosphere of Mars produces suprathermal atoms, which populate hot atomic oxygen, nitrogen, and carbon exospheric coronae [*McElroy*, 1972; *Nagy and Cravens*, 1988; *Lammer and Bauer*, 1991; *Kim et al.*, 1998; *Johnson and Luhmann*, 1998; *Hodges*, 2000, 2002; *Lammer et al.*, 2003; *Krestyanikova and Shematovich*, 2005; *Fox and Hać*, 2009, 2014; *Valeille et al.*, 2009a, 2009b, 2010a, 2010b; *Gröller et al.*, 2014; *Lee et al.*, 2015a, 2015b; *Deighan et al.*, 2015; *Rahmati et al.*, 2015; *Lillis et al.*, 2015]. A hot oxygen corona was observed at Venus by measurements of resonantly scattered solar photons in the OI 130.4 nm line made by the ultraviolet spectrometer on board the Pioneer Venus Orbiter [*Nagy et al.*, 1981, 1990] and now has also been observed at Mars [*Deighan et al.*, 2015]. Hot O is produced by the dissociative recombination (DR) of the major ion species in the ionosphere, O_2^+ [*McElroy*, 1972; *Nagy et al.*, 1981, 1990; *Nagy and Cravens*, 1988]:

$$\begin{aligned} O_2^+ + e &\rightarrow O(^3P) + O(^3P) + 6.96\ \text{eV} \quad (0.22) \\ &\rightarrow O(^3P) + O(^1D) + 5.00\ \text{eV} \quad (0.42) \\ &\rightarrow O(^1D) + O(^1D) + 3.02\ \text{eV} \quad (0.31) \\ &\rightarrow O(^1D) + O(^1S) + 0.80\ \text{eV} \quad (0.05) \end{aligned} \tag{1}$$

Note that the O escape energy near an altitude of 200 km is $E_{esc} \approx 2$ eV, so that the first two branches of reaction (1) produce O atoms that have sufficient energy to escape the planet and atmosphere. Each O atom is produced with close to half the exothermic energy due to momentum conservation. Branching ratios adopted for the reaction products have varied, but the values currently assumed by most modelers [see *Fox and Hać*, 2009] are provided in equation (1) and are shown in the parentheses. The DR rate coefficient [*Peverall et al.*, 2001; *Petrignani et al.*, 2005] is given by $\alpha = 2 \times 10^{-7}\ \text{cm}^3\ \text{s}^{-1}\ (300\ \text{K}/T_e)^{0.7}$, where T_e is the

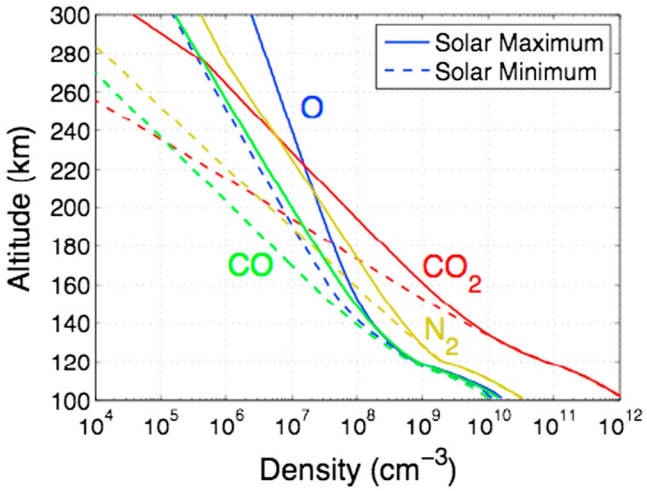

Figure 1. CO_2, CO, O, and N_2 density profiles for the Martian thermosphere for solar minimum and maximum conditions. From MGITM model [*Bougher et al*., 2015a] and used by *Rahmati et al*. [2014, 2016]. These densities agree overall with the initial measurements of the density by the NGIMS instrument on board MAVEN [*Mahaffy et al*., 2015]. The local time assumed is 11:00.

electron temperature. T_e in the Martian ionosphere varies from about 300 K up to about 5000 K [*Chen et al*., 1978; *Hanson and Mantas*, 1988; *Matta et al*., 2014; *Ergun et al*., 2015; *Sakai et al*., 2016]. The O_2^+ DR reaction also produces hot O at Earth [e.g., *Yee et al*., 1980; *Kharchenko et al*., 2000].

Hot O, or other atoms, can also be produced by other ionospheric chemical reactions, including charge exchange of hot ions with neutrals (e.g., $O^+ + H \rightarrow O_{fast} + H^+$) or DR of CO_2^+ ions [*Gröller et al*., 2014], but these are minor sources at Mars. At Venus and Earth, all the hot O atoms produced by the DR reaction have speeds less than the escape speed and the exospheric O atoms remain in bound orbits.

The atoms produced by the top two reaction channels in equation (1) have speeds greater than the $v_{esc} = 5$ km/s escape speed for Mars and can escape the planet if they are produced in the exosphere (see references above). This has been shown to be an important loss process for Mars and a source of a hot O corona [e.g., *Nagy and Cravens*, 1988; *Kim et al*., 1998; *Fox and Hać*, 2014]. A variety of models have been constructed to study the hot atom coronae (and escape) of Venus, Mars, and Titan (see earlier references) using different methods. Fast oxygen atoms produced by various means, but especially from DR, mainly collide elastically with ambient atoms and molecules resulting in changes in direction and energy loss (or gain) that alter the trajectories of the O atoms. Such collisions cool the O atoms on average and, if the altitude is low enough (i.e., below the so-called "traditional exobase"), prevent them from reaching the exosphere and thus escaping if they have enough energy (i.e., 2 eV). However, atoms produced at high enough altitudes can populate the exosphere/corona. The collision process has been modeled with methods like the two-stream method or Monte Carlo methods, and a variety of cross sections for O collisions with CO_2, O, and other species have been adopted over the years [see *Lillis et al*., 2015, and above references], none of which are entirely satisfactory. Figure 1 shows the neutral density profiles in the Martian thermosphere for different solar activity levels, based on the Mars Global Ionosphere-Thermosphere Model (MGITM) [cf. *Bougher et al*., 2015a].

In spite of the large numbers of numerical models of hot O at Mars, a number of issues remain, two of the key ones (but not the only ones) being (1) How do oxygen escape rates scale with the solar ultraviolet irradiance, both now and in the geological past? and (2) What elastic cross sections should be used in hot O calculations and how are escape rates affected by the choice of cross section [e.g., *Fox and Hać*, 2014]? Measurements of ionospheric and atmospheric properties of Mars by the Mars Atmosphere and Volatile Evolution (MAVEN) spacecraft are well underway, and the first observations of the Martian hot oxygen corona have been made [*Deighan et al*., 2015; *Lee et al*., 2015a, 2015b; *Rahmati et al*., 2015]. Comparison of this hot O data with models should soon lead to improvements in our understanding of this subject and help to answer these two questions.

It makes sense that oxygen escape rates and exospheric densities associated with photochemistry should scale linearly with EUV irradiance. This should remain true if the basic atmospheric composition remains the same for the different solar conditions, but the *Zhao and Tian* [2015] model indicated that for EUV irradiances more than 10 times current values the O escape rate actually decreases. This was attributed to an increasing fraction of atomic species rather than molecular species in the upper atmosphere due to increased photodissociation rates.

The purpose of the current paper is to develop a simple (but hopefully not oversimplified) analysis of O escape, in order to clarify the dependencies on solar irradiance and on cross sections. Correlations and

assumptions sometimes get buried in a numerical model so analytic expressions for photochemical loss of O and for ion loss will be derived and discussed. The derived expressions are not meant to replace detailed numerical models, which are still needed, but will hopefully help advance the discussion of model results and their relation to MAVEN data.

2. Ionospheric Chemistry

The major neutral species in the thermosphere of Mars is CO_2, although atomic oxygen is the major neutral species at higher altitudes (i.e., above about 200–250 km depending on solar activity level) [*Bougher et al*., 2015b, 2015c; *Mahaffy et al*., 2015]. Ions and photoelectrons are created on the dayside via photoionization of neutrals by solar EUV and soft X-ray radiation:

$$\begin{aligned} h\nu + CO_2 &\rightarrow CO_2^+ + e \\ h\nu + O &\rightarrow O^+ + e \end{aligned} \tag{2}$$

Secondary ionization by photoelectrons also contributes about 10% to the total ionization rate. CO^+ ions are produced by photoionization of CO or by dissociative ionization of CO_2, and N_2^+ and N^+ ions are produced from ionization of N_2. The production rate of photoions can be calculated using standard aeronomical techniques. Figure 3 shows the total ion production rate profiles due to solar radiation including all ion species and including both primary and secondary ionization. The methods and inputs, including photoionization and photoabsorption cross sections, are described by *Sakai et al*. [2015]. The neutral densities used in the calculations were those shown in Figure 1 for solar maximum and the solar irradiance used for moderately high solar activity ($F_{10.7} \approx 130$). A very useful indicator of solar irradiance (or activity) is the solar radio flux at 10.7 cm (2800 MHz) because it has been in use for a very long time and is commonly used. We will use the $F_{10.7}$ index in our paper as a measure of solar activity.

CO_2^+ ions mainly react with atomic oxygen to produce O_2^+ ions:

$$CO_2^+ + O \rightarrow O_2^+ + CO \tag{3}$$

Below about 250 km, O^+ ions mainly react with CO_2 to produce O_2^+ ions [cf. *Fox*, 1993; *Chen et al*., 1978]:

$$O^+ + CO_2 \rightarrow O_2^+ + CO \tag{4}$$

The Viking 1 and 2 retarding potential analyzer experiments showed that O_2^+ was the main ion species below about 250 km [*Hanson et al*., 1977]. The CO_2^+ density is about 10% of the O_2^+ density near an altitude of 200 km. This has been observationally confirmed by measurements made by the Neutral Gas and Ion Mass Spectrometer (NGIMS) experiment on board the MAVEN spacecraft [*Benna et al*., 2015].

The main ionospheric loss process is dissociative recombination (DR) of O_2^+, although DR of CO_2^+ also takes place and contributes to some hot O production (see equation (1)). Note that CO^+ or O^+ produced by DR of CO_2^+ also becomes O_2^+ via ion-neutral chemistry and is automatically included in the hot O production rate discussed in the later sections. Most of the N_2^+ ions produced become CO_2^+ ions via the following fast reaction:

$$N_2^+ + CO_2 \rightarrow CO_2^+ + N_2 \tag{5}$$

The CO_2^+ mostly continues on to become O_2^+, although some CO_2^+ dissociatively recombines, producing hot O. Ionospheric chemistry at Mars is discussed in several papers [*Schunk and Nagy*, 2009; *Fox et al*., 2015; *Ergun et al*., 2016], and the reader is referred to them for details on the chemistry. *Schunk and Nagy* show a "flow diagram" for the Venus and Mars ionospheric chemistry, and some readers might find this useful.

N_2^+ mainly reacts with O to become NO^+, which then dissociatively recombines, producing fast N and O atoms. CO^+ ions react with CO_2 to produce CO_2^+ ions and then O_2^+. Hence, for the most part, almost any ion produced from any neutral species will end up as O_2^+, as long as there is sufficient CO_2 and O to react with. Current ionospheric models can explain the observed major ion composition [*Fox et al*., 2015; *Benna et al*., 2015; *Withers et al*., 2015…], but there is also a rich minor ion chemistry [cf. *Matta et al*., 2013; *Fox et al*., 2015], which we will not discuss.

Table 1. Solar Ionization Frequencies (1 AU) and Collision Cross Sections for Atomic Oxygen and for Solar Minimum and Maximum Conditions[a]

Species j	I (Max)	I (Min)	σ_{0-j}	b_j (Max)	b (Min)
CO_2	17.7[b]	6.04[b]	13[c]	1.41[d]	0.48[d]
CO	11.2	3.87	9.7	1.12	0.40
O	7.01	2.28	2.5	2.78	0.90
N_2	8.22	3.06	9.7	0.85	0.32

[a]Min and max refer to the solar minimum and maximum values.
[b]Units of 10^{-7} s^{-1}.
[c]Units of 10^{-16} cm^2. Effective backscatter cross sections of O with species r are shown.
[d]Units of 10^{9} cm^{-2} s^{-1}.

3. Photochemical Hot Oxygen Production and Escape

O atoms produced by DR of O_2^+ or CO_2^+ are suprathermal and populate a hot oxygen exosphere or corona (see section 1 for references). Two of the DR loss channels of O_2^+ are such that the velocity of the O can exceed the escape speed at Mars ($v_{esc} = 5$ km/s or O energy of 2 eV). A detailed analysis of the production takes into account the translational and vibrational energies of the O_2^+ ions [*Fox and Hać*, 2009, and references therein]. About half the O produced (64%) [*Fox and Hać*, 2009] by DR exceeds the escape energy, and two O atoms are produced per DR reaction (see equation (1)):

$$P_O(z) = 2\ \alpha\ n_e\ n_{O2+} \tag{6}$$

n_e is the electron density and n_{O2+} is the O_2^+ density. Overall, the fraction of the total DR rate that goes to O atoms with energies greater than the escape energy is about 1. We thus introduce an efficiency factor $f = 1$. In the main ionosphere $n_e \approx n_{O2+}$, but at higher altitudes in the topside ionosphere $n_e \approx n_{O2+} + n_{O+}$. In this paper, we assume that the ion loss (e.g., equation (6)) equals ion production (that is, assumption of photochemical equilibrium) and approach the loss rate reaction (6) via the production rate side (i.e., equation (2)).

O atoms produced at altitudes where the neutral density is high will collide with ambient neutral species (mainly CO_2 but also CO, N_2, and O), preventing them from escaping, although they contribute to heating the atmosphere. Collisional processes for hot atom coronae have been studied at both Venus and Mars (references cited in section 1), and the methods include the two-stream method, diffusion methods, and Monte Carlo methods. For an escaping O atom a single large-angle collision will prevent its escape (and the subsequent O atom will be directed back downward and/or no longer have sufficient energy to escape). The escape probability as a function of altitude, G_{esc}, can then be written as

$$G_{esc}(z,\theta) = \exp[-(\sigma_{OO}N_O + \sigma_{OCO2}N_{CO2} + \sigma_{ON2}N_{N2} + \sigma_{OCO}N_{CO} + \ldots)\sec\theta] \tag{7}$$

The angle of an escaping oxygen velocity vector with respect to the radius vector (i.e., vertical) is denoted θ. N_O is the vertical neutral oxygen column density above altitude z (i.e., integral of the O density over altitude), and N_{CO2} is the same for CO_2, and the same is true for the other species. σ_{OO}, σ_{OCO2}, σ_{ON2}, and σ_{OCO} are the backscatter (not total) elastic cross sections for O collisions with O, CO_2, N_2, and CO target species, respectively. Considering the densities in Figure 1, just keeping the O and CO_2 terms is a good first approximation (albeit somewhat subject to solar conditions). At an altitude of 200 km CO_2 provides most of the collisional opacity, but N_2 does account for a sizable ≈ 20%. The CO contribution is not important.

Experimental and theoretical information on the elastic cross sections needed in hot O models is scarce, and most recent modelers have used the O-O differential cross section calculated theoretically by *Kharchenko et al.* [2000] and have then scaled these cross sections to other target species. Different modelers have handled the forward scattering peak in the Kharchenko cross section differently. This is somewhat less important if one just focuses on escape and not on finding the full O energy and altitude distributions. Simply integrating the Kharchenko O-O cross section in the backscatter direction gives a cross section of $\sigma_{O\text{-}O} = 3.8 \times 10^{-16}$ cm^2. *Rahmati et al.* [2014] used a value of 2.5×10^{-16} cm^2 (Table 1), but many other values can be found in the literature. Most modelers use the full differential cross section of *Kharchenko et al.* [2000], although they handle the forward peak differently. Using Table 1 cross sections and the solar maximum

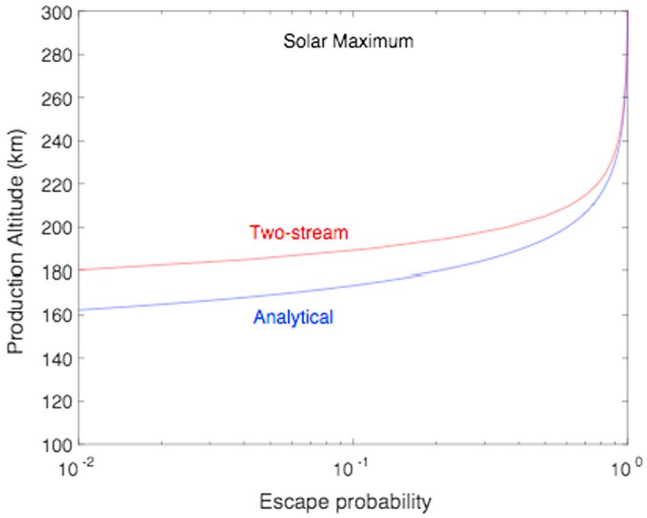

Figure 2. Oxygen escape probability as a function of altitude and exit angle of 60° are shown for the solar maximum neutral atmosphere shown in Figure 1. Comparison escape fractions from the numerical two-stream model of *Rahmati* [2016] are shown for comparison.

atmosphere from Figure 1 gives the results shown in Figure 2 for an exit angle of 60° with respect to the vertical.

4. Production of the Ionosphere by Solar Radiation

A short synopsis of standard aeronomy [e.g., *Schunk and Nagy*, 2009] in a form needed to determine the O escape rate is now discussed. The production rate of ions of species *s*, due to photoionization of neutral species, *s*, by solar radiation is given by

$$P_s(z) = \sum_{\lambda} F_{\lambda}(z)\sigma_{s,\mathrm{ion}}(\lambda)n_s(z) \quad (8)$$

where F_λ is the solar flux at altitude z and at wavelength λ, $n_s(z)$ is the density of neutral species s at altitude z, and $\sigma_{s,\mathrm{ion}}$ is the photoionization cross section for species s at photon wavelength λ. In our case the most important species being ionized are CO_2 and O, particularly the former. For the current paper we do not keep track of the ion final state in the photoionization process, although the model that produced Figure 3 did include this effect.

The solar flux at altitude z is given by

$$F_\lambda(z) = F_{0\lambda}\exp(-\tau_\lambda(z)) \quad (9)$$

where τ_λ is the optical depth at z and for wavelength λ and $F_{0\lambda}$ is the solar flux at the top of the atmosphere. The optical depth can be approximated for solar zenith angles that are not too close to 90° by the expression:

$$\tau_\lambda = \sec(\chi)\sum\nolimits_s \sigma_{\mathrm{abs},s}(\lambda)N_s(z) \quad (10)$$

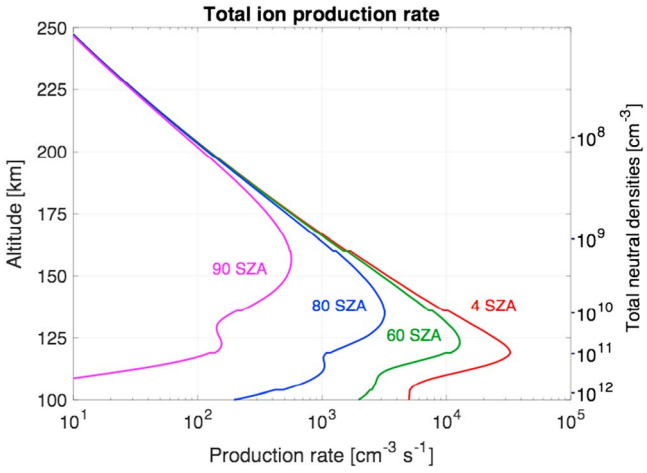

Figure 3. Total ion production rate (all ion species and both primary and secondary ionization) vertical profiles for solar EUV radiation for the MAVEN epoch. The approximate $F_{10.7}$ index of solar activity is 130. The same model and neutral atmosphere as used by *Sakai et al.* [2016] was used, although Sakai et al. did not show ion production rates. Results for several solar zenith angles are shown and an approximate exobase altitude is 200 km.

$N_s(z)$ is the vertical column density of species s at altitude z, and $\sigma_{\mathrm{abs},s}(\lambda)$ is the photoabsorption cross section at wavelength λ for species s:

$$N_s(z) = \int_z^{\infty} n_s\left(z'\right)dz' \quad (11)$$

The ionization frequency due to photoionization by solar radiation for species s in the optically thin region is given by $I_s = P_s\ (z)/n_s(z)$ and is independent of altitude. Note that Table 1 lists some ionization frequencies for both solar minimum and maximum conditions and a heliocentric distance of 1 AU [*Cravens et al.*, 1987]. *Schunk and Nagy* [2009] also provide ionization frequencies. The values for Mars should be about half these values due to its larger heliocentric distance. Figure 3 shows the modeled total ion (CO_2^+, CO^+, O^+, N_2^+…) production rate profiles at Mars

for typical 2015 MAVEN solar conditions and the solar maximum neutral atmosphere shown in Figure 1. Information on photoionization and photoabsorption cross sections and on solar irradiances for this epoch can be found in *Sakai et al.* [2015, 2016]. Results for four solar zenith angles are shown. Secondary ionization (i.e., ionization by photoelectrons) as well as primary ionization were included. Note that Figure 3 illustrates that optical depth effects are not important above about 160 km, even at the terminator, well below altitudes where the escape rate is significant. The species-averaged ionization frequency for the MAVEN epoch and for Mars from Figure 3 is $\approx 8\times10^{-7}\,s^{-1}$, which is consistent with Table 1 (which has 1 AU values and is for solar maximum).

A rough approximation to the ion production rate that somewhat improves upon the optically thin approximation is

$$P_s(z)\approx I_s n_s(z)\exp\left[-<\sigma_{abs,CO2}>N_{CO2}(z)\sec\chi\right] \tag{12}$$

where an "effective" wavelength-averaged cross section is used. For CO_2 at a "typical" EUV wavelength of about 50 nm, $<\sigma_{abs,CO2}>\approx 3\times10^{-17}\,cm^2$. We do not really use this approximation except to demonstrate that optical depth effects are not important for oxygen escape.

5. Simple Oxygen Escape Model

5.1. CO_2 Targets

The photochemical solution for the electron density in the ionosphere comes from neglecting transport and setting production equal to chemical loss. See *Schunk and Nagy* [2009] for an explanation of such basic aeronomical processes. For O_2^+ at Mars, the appropriate equation can be approximated by $P_{CO2+}\approx\alpha n_e^2$, assuming that most of the photoionization is from CO_2 and that O_2^+ is the major ion species. The O production rate is twice P_{CO2+} (equation (8)). The fraction of O atoms produced that exceed the escape energy is about half of the total produced. All these factors can be included in a parameter, f, which should be very close to unity: $f\approx 1$. f is a production efficiency factor. The production of oxygen atoms that can potentially escape is given by

$$P_{esc,\ O}(z) = f\ \ P_{CO2+} \tag{13}$$

The hot O escape rate from the top of the atmosphere is the integral over altitude of this production rate multiplied by the probability that an upward moving oxygen atom can escape the atmosphere. Hence, we must also integrate over upward emission angles ($0<\theta<90°$). Rearranging the expressions given earlier gives the following equation:

$$\begin{aligned} F_{esc,O} &= \frac{1}{4\pi}\int_0^\infty dz' \int_0^{\pi/2} P_{esc,O}\left(z'\right) G_{esc}\left(z',\theta\right) 2\pi\sin\theta d\theta \\ &= \frac{1}{4\pi}\int_0^\infty dz'\, n_{CO2}\left(z'\right) \int_0^{\pi/2} f I_{CO2}\exp\left[-<\sigma_{absCO2}>\sec\chi N\left(z'\right)\right]\exp\left[-\sigma_{OCO2}N\left(z'\right)\sec\theta\right] 2\pi\sin\theta d\theta \end{aligned} \tag{14}$$

Equation (14) can be easily integrated over z' by recognizing that $dN_{CO2}=n_{CO2}dz'$:

$$F_{esc,O} = \frac{f I_{CO2}}{4\pi}\int_0^{\pi/2}\frac{2\pi\sin\theta d\theta}{<\sigma_{absCO2}>\sec\chi+\sigma_{OCO2}\sec\theta} \tag{15}$$

Given that $\sigma_{OCO2}\approx 10<\sigma_{absCO2}>$, the first term in the denominator can be neglected, and the integral over θ in equation (15) carried out to give

$$F_{esc,O}\cong\frac{f I_{CO2}}{4\sigma_{CO2}} \tag{16}$$

with $f\approx 1$. This escape flux is independent of the location on the dayside of Mars except in the immediate vicinity of the terminator. Hence, the global escape rate of O is $2\pi R_M^2$ times this flux or

$$Q_{esc,O} = \left(f\ \ I_{CO2}\ \ \pi R_M^2/2\sigma_{OCO2}\right) \tag{17}$$

Note that equation (16) could also have been obtained using a standard "exobase" approximation, with exobase defined as where the collisional depth equals unity ($1 \approx 2\ \sigma_{OCO2}\ N_{CO2}$ with vertical column density given by $N_{CO2} \approx n_{exo}\ H_n$):

$$n_{exo} \approx 1/(2\sigma_{OCO2}\ H_n) \tag{18}$$

where $H_n = kT_n/m_{CO2}g$ is the neutral scale height. However, we did not need to make an explicit exobase assumption in deriving our equations.

5.2. Escape Estimate With O, N_2, CO, and CO_2 Included in the Thermosphere

A somewhat improved escape flux estimate can be obtained if one also includes other target species such as atomic oxygen, N_2, and CO as well as CO_2, as long as the atmosphere is optically thin to incoming solar ionizing radiation. We now include ionization of these species leading to the production of O^+, N_2^+, CO^+, etc. (assumed to come from photoionization of the respective neutral species). We still assume that all such ion species produced are consumed locally and produce O_2^+ ions, which in turn produces hot O atoms via DR. We discuss this questionable assumption later. We also allow other neutral species to collisionally impede the escape of hot O.

The total production rate of O_2^+ is now given by $P_{ion} = P_{CO2+} + P_{O}^+ + P_{CO}^+ + P_{N2}^+$, wherein the optically thin region, $P_{O}^+ = I_O n_O$, $P_{CO2+} = I_{CO2} n_{CO2}$, etc. The new production rate of potentially escaping O is given by $P_{esc,O} = f\ P_{ion}$. By using the total ion production rate for all species we are assuming that all ion species produced end up as O_2^+ ions and thus lead to hot O atoms (or to another ion species that can lead to hot O atoms).

The escape fraction, $G_{esc}(z)$, now includes the effects of O collisions with all neutral species, which requires that all the effective backscatter cross sections be included in the original equation (7). Define the ratio of the ionization frequency of species s to that species' effective backscatter cross section for O collisions as $b_s = I_s/\sigma_{Os}$. Denote the value of this ratio for species $s = CO_2$ as b_1. If all the values of $b_s = b_1$ then for the purposes of the escaping O flux, all neutral species are equivalent and the escape flux does not depend on neutral composition or on the altitude dependence of the neutral density. The simple analytical solution given by equation (16) still applies, although it can be written as $F_{esc,O} = f\ b_1/4$. Equation (17) still applies also. Uncertainties should be no more than the range of the values of the b coefficients in Table 1 (that is, about a factor of 2).

6. Comparison of the Simple Escape Model With a Numerical Model

Rahmati et al. [2014, 2016] and other researchers (see section 1 for references) calculated hot oxygen density profiles and oxygen escape rates. *Rahmati et al.* [2015] also determined the fluxes of oxygen ions picked up by the solar wind far upstream of Mars and associated with the distant neutral O corona. As indicated in the introduction *Rahmati et al.* used a two-stream O transport model in their calculations, as did *Nagy and Cravens* [1988] and *Kim et al.* [1998] (albeit with different elastic scattering cross sections). *Rahmati* also used Monte Carlo collision methods to verify that the two-stream method was accurate, which it was. Other methods have also been applied to the hot O distribution and escape rate problem [*Fox and Hać*, 2014; *Lee et al.*, 2015a, 2015b]. Key ingredients in these calculations are the oxygen-scattering cross sections for collisions with ambient neutral species, particularly CO_2, but also CO, O, and N_2. Unfortunately, not much information is available for the relevant cross sections. *Fox and Hać* [2014] used a cross section of 3×10^{-15} cm^2 for 11 different neutral species and worked with an isotropic scattering model and a forward-scattering scattering model in which the *Kharchenko et al.* differential scattering cross section was used to set the differential scattering cross section for all species. They concluded that the forward scattering cross section should be most useful. Later in the paper, results from this paper are shown together with results from other models.

For our simple escape formula we used the backscatter cross section and assumed that only a single collision renders the O atom incapable of escape, because a second collision would be needed to redirect the atom upward and sufficient energy would be lost to lower the energy below the escape energy.

Rahmati (PhD thesis, 2016) [also see *Rahmati et al.*, 2014] used backscatter cross sections for different species (i.e., total elastic cross section plus the backscatter probability), and we will adopt these values here as listed in Table 1. Table 1 also shows the solar radiation photoionization frequencies for solar minimum and maximum for several species and for a heliocentric distance of 1 AU [*Cravens et al.*, 1987], the effective backscatter

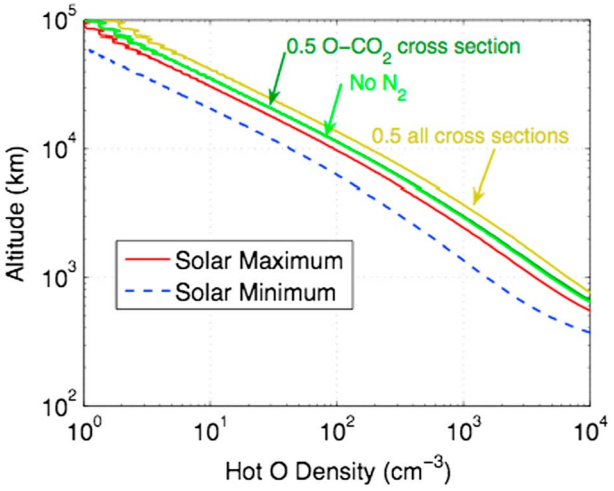

Figure 4. Hot O densities versus altitude from the two-stream hot O model (see *Rahmati et al.* [2014, 2017]). Density profiles for the standard solar model for solar maximum and minimum are shown. Model profiles for a case with half the O-CO_2 cross section and with half all cross sections (including O-O and O-CO and O-N_2). The densities for the last case are indeed about a factor of 2 higher than for the standard model, as are the escape fluxes discussed in the text.

cross sections just mentioned. Note that when we apply these frequencies to Mars, we need to also include (1) about a 10% enhancement due to secondary ionization (i.e., photoelectrons) and (2) a factor accounting for the heliocentric distance of Mars (i.e., a solar flux reduction of ≈0.43). We just lump these extra factors into an effective f value (i.e., $f_{\mathrm{eff}} = 1.1\ f/d^2 \approx 0.4$, where d is the heliocentric distance of Mars in units of AU). Note that this heliocentric distance depends on where Mars is located in its orbit (i.e., seasonal progression). Table 1 also lists the b ratios for each target species.

Now we can carry out simple escape estimates using the b value from Table 1 just for CO_2. However, these values are different for different species, which does violate our assumption by about a factor of 2. We push ahead, though, with just the CO_2 values. The escape fluxes of O from $F_{\mathrm{esc,O}} \approx f_{\mathrm{eff}}\ b_1/4$ are

$$\begin{aligned} &F_{\mathrm{esc,O}} \approx f_{\mathrm{eff}}\ \ b_1/4 = (0.4/4)\ \ b_1 = 0.1\ \ b_1 \\ &F_{\mathrm{esc,O}} \approx 1.4\times10^{8}\ \ \mathrm{cm}^{-2}\ \ \mathrm{s}^{-1}\ \ \text{for solar maximum}\quad \left(Q_{\mathrm{esc,O}} \approx 8.8\times10^{25}\ \ \mathrm{s}^{-1}\ \ \text{global}\right) \\ &F_{\mathrm{esc,O}} \approx 4.8\times10^{7}\ \ \mathrm{cm}^{-2}\ \ \mathrm{s}^{-1}\ \ \text{for solar minimum}\quad \left(Q_{\mathrm{esc,O}} \approx 3.0\times10^{25}\ \ \mathrm{s}^{-1}\ \ \text{global}\right) \end{aligned} \tag{19}$$

The $F_{10.7}$ index of solar activity was about 120 for the first year of the MAVEN mission—neither a solar minimum value nor a typical solar maximum value. The solar maximum escape fluxes from equation (19) should be adjusted downward by the approximate $F_{10.7}$ ratio of 120/200 = 0.6, which gives $F_{\mathrm{esc,O}} = 8.4\times10^{7}\ \mathrm{cm}^{-2}\ \mathrm{s}^{-1}$ and $Q_{\mathrm{esc,O}} = 5.3\times10^{25}\ \mathrm{s}^{-1}$.

Compositional uncertainties affect the results to the degree that the b values are different—O targets allow more escape, and N_2 targets allow less escape than CO_2. Again, all this is subject to the more basic assumption of photochemical equilibrium.

The *Rahmati et al.* [2014] and *Rahmati* [2016] numerical model gave an escape rate of $9.1\times10^{7}\ \mathrm{cm}^{-2}\ \mathrm{s}^{-1}$ for solar maximum and $4\times10^{7}\ \mathrm{cm}^{-2}\ \mathrm{s}^{-1}$ for solar minimum. This model included O and N_2 collisions and used MGITM ionization rates. Note that the solar maximum to solar minimum escape flux ratio depends simply on the ratio of the input solar fluxes in both cases, which is as expected. *Rahmati et al.* also numerically calculated O density profiles (including both bound and escaping O atoms) as shown in Figure 4. These density curves also scale with the b value, although in the current paper we only consider escape fluxes.

7. Ion Transport and the Photochemical Equilibrium Assumption

For completeness, in this section we roughly assess the contribution of ion transport to atmospheric loss but leave a more thorough discussion of this topic to a large number of other papers (see the references provided by *Brain et al.* [2015]). The photochemical O escape analysis undertaken earlier in our paper assumed that ionization locally produced is locally lost and is channeled into hot oxygen via DR of O_2^+. However, it is known that ion transport processes become important for ionospheric plasma at high enough altitudes on any planet, and this will also be true for Mars [e.g., *Fränz et al.*, 2010; *Ma et al.*, 2015; *Brain et al.*, 2015; *Ergun et al.*, 2016]. The flow is mainly from day to night and removes plasma from the dayside ionosphere and supplies it to the nightside and/or to the wake region [cf. *Fox*, 1993, 1997, 2009; *Fränz et al.*, 2010; *Brain et al.*, 2015], although some plasma can also exit the planet in the polar plume [e.g., *Dong et al.*, 2014]. Ions

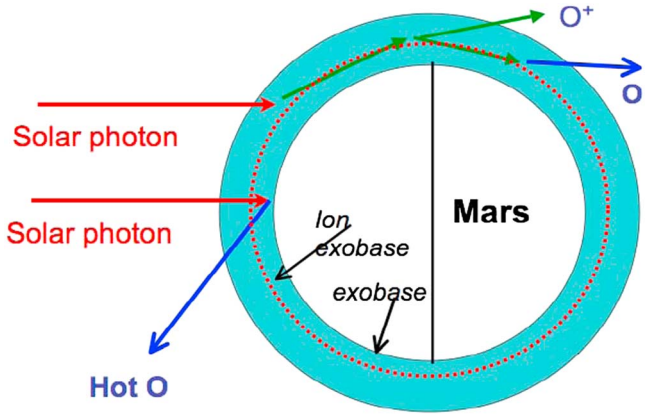

Figure 5. Schematic of the Martian upper atmosphere and ionosphere, illustrating the exospheric region where photochemical O production takes place and the region of ion loss from day to night above the ion exobase. Note that we did not use an explicit exobase approximation in the calculations.

entirely removed from the dayside ionosphere by transport are not available for local dayside photochemical loss but still represent an atmospheric loss (although with a label of "ion loss"). Figure 5 is a schematic illustrating the photochemical and ion loss regions at Mars.

The transition between the photochemically controlled ionosphere and a transport-dominated ionosphere can be estimated by comparing the plasma transport time (τ_T) to the photochemical lifetime of the major ion species. MAVEN ionospheric data [e.g., *Mahaffy et al.*, 2015; *Benna et al.*, 2015] and ionospheric models of Mars [e.g., *Withers et al.*, 2015] indicate that under most circumstances, O_2^+ remains the major ion species up to about 300 km. The chemical lifetime of O_2^+ is given by the dissociative recombination time: $\tau_{DR} = 1/(\alpha n_e)$. O^+ ions react with CO_2, N_2, or H and have the relevant ion-neutral time scale, which is inversely related to the neutral density. We will focus on O_2^+, which remains a major ion throughout the topside ionosphere. Evaluating the DR coefficient with an electron temperature of 3000 K gives the DR time constants listed in Table 2. Typical values of n_e (which must equal the total ion density, n_i, due to quasineutrality) and n_n are taken from published data from the NGIMS instrument on MAVEN [*Mahaffy et al.*, 2015]. The values used in our estimates are roughly consistent with Langmuir probe data [*Ergun et al.*, 2015] and models for comparable solar activity levels.

The expression for τ_{DR} can be made more general than those listed in Table 2 by using a photochemical equilibrium expression for the electron density. The photochemical continuity equation for O_2^+ ions (and electrons) is

$$P(z) = I_O \; n_n(z) = \alpha \; {n_e}^2 \tag{20}$$

Using standard aeronomical methods, equation (20) can be solved for the electron density:

$$n_e \approx (I_O/\alpha)^{1/2} {n_n}^{1/2} \tag{21}$$

The ionization frequency of oxygen (I_O) was used here, because in the topside ionosphere (above 200 km or so), O becomes the most important neutral species. Note that I_O depends on the incident solar EUV irradiance. This expression can be written as (for $T_e \approx 3000$ K)

$$n_e(\mathrm{cm}^{-3}) \approx 3.3 \; {n_n}^{1/2} (F10.7/200)^{1/2} \tag{22}$$

At 300 km where $n_n = 3 \times 10^6\,\mathrm{cm}^{-3}$ (Table 2), and for $F_{10.7} \approx 120$, equation (22) gives $n_e \approx 4.4 \times 10^3\,\mathrm{cm}^{-3}$, whereas the value quoted in Table 2 is a bit different at $\approx 2 \times 10^3\,\mathrm{cm}^{-3}$. However, only estimates are being considered here. $F_{10.7}$ is a convenient and readily available proxy for solar EUV irradiance, but other proxies could also be used in equation (22).

Table 2. Topside Ionosphere Flow Speeds and Transport Times

Alt (km)	n_n (cm^{-3})	n_e (cm^{-3})	τ_{DR} (s)	τ_T (s)
200	1.5×10^8	2×10^4	500	6×10^4
250	3×10^7	7×10^3	1500	5×10^3
300	3×10^6	2×10^3	5000	10^3
350	1×10^6	10^3	10^4	2×10^2

In order to estimate the transition from photochemical control of the ionosphere to transport control we can compare the chemical lifetime with the transport time (where $\tau_T \approx \tau_{DR}$), all as functions of neutral density, and then find this critical, or transition, neutral density (n_{nc}). The transport time, τ_T, is

roughly an appropriate length scale, L, divided by the plasma flow speed, u. That is, $\tau_T \approx L/u$. When a magnetic field with a significant radial component is present (e.g., near the edges of crustal magnetic field regions), then the transport could be dominated by ambipolar diffusion along the magnetic field.

A detailed consideration of plasma dynamics is beyond the scope of the current paper. There is a large literature on the solar wind interaction with Mars and its plasma environment, but there is little detailed information on the plasma flow in the ionosphere itself. Outside the crustal magnetic field regions, magnetic fields are induced in the Martian ionosphere and drive flow (together with thermal pressure gradients) mainly from day to night and with relatively low radial speeds. The length scale should be a typical "day to night" distance ($L \approx R_M/2$). Flow speeds should go from low values deep in the ionosphere, where the plasma is tied to the neutral winds, up to higher values in the magnetic pileup region and very high values in the magnetosheath. That is, as the neutral density decreases, the flow speed should increase.

Cravens et al. [2010] carried out simple estimates of the ionospheric flow speed in Titan's ionosphere in which pressure forces (mainly magnetic pressure) was balanced by ion-neutral collisions. They derived very simple, and very rough, expressions for the ion flow speed and transport time, using this ambipolar diffusion approximation: $\tau_T \approx L^2\, n_e\, m_i\, k_{\mathrm{in}}\, n_n/p_B$, where $L \approx R_M/2$ is a horizontal length scale, n_e is the electron density, n_n is the neutral density, k_{in} is the ion-neutral collision frequency coefficient, and p_B (≈1 nPa at Mars) is the ionospheric magnetic pressure which we take to be a typical solar wind pressure. Table 2 lists some rough time scales from this approach, but in the future more effort should be devoted to making better estimates using global numerical models [cf. *Ma et al*., 2015] and/or more sophisticated analytical models. The transition density/altitude should be quite variable given that the solar wind is variable.

In lieu of a detailed knowledge of plasma flow speeds in the ionosphere, we take a shortcut and look at the extensive ionospheric electron density (and now with MAVEN ion density) data to see at what typical altitude (and thus neutral densities) dayside plasma density profiles show departures from simple exponential behavior characteristic of photochemical behavior. Some authors call this boundary the "ionopause" [e.g., *Vogt et al*., 2015], although they point out that these ionopauses are not pressure-balance ionopauses like those observed in the Venus ionosphere [cf. *Luhmann and Cravens*, 1991]. A cursory examination of ionospheric data can perhaps indicate at what altitude electron density (or ion density) profiles look anomalous (i.e., not exponential or exponential with a drastically different scale height from lower altitudes). A large number of papers in the special issue of a 2015 *Geophysical Research Letters* devoted to MAVEN results are relevant to this issue. In particular, the *Vogt et al*. paper seems to show that although the ionopause altitude is quite variable, as expected, 280–320 km appears to be a transition altitude of some type on average. The neutral density at this altitude ($n_{\mathrm{nc}} \approx 3 \times 10^6\ \mathrm{cm}^{-3}$) we identify as the critical altitude above which ions are likely to be affected by transport and transport loss (Table 2 or Figure 1).

As discussed earlier, ionospheric plasma transported from the dayside can either supply the nightside ionosphere or the ions can be lost to Mars via "ion escape" out the tail or in the ion plume [cf. *Brain et al*., 2015]. Ions that cross into the nightside and drift downward are ultimately lost via DR of O_2^+ deeper in the ionosphere, sometimes again leading to O escape. Either way most of the ionization produced in the transport region (i.e., above the critical density, n_{nc}, altitude) is still associated with atmospheric loss of O and other species.

The supply of ions for the ion escape is limited to neutrals that can be ionized in the transport region by solar radiation (or by impact ionization due to external electron/ion precipitation). This "production-limited" concept was discussed by *Ergun et al*. [2006]. The global dayside ion loss rate due to this high-altitude ionization can very roughly be expressed in terms of the critical neutral density, making it somewhat independent of the detailed neutral density profiles (and exospheric neutral temperature):

$$Q_{\mathrm{esc,O}} \approx 2\pi\ R_M{}^2 I_O\ n_{\mathrm{nc}} H_n \approx 2.5 \times 10^{24}\ \mathrm{s}^{-1} \tag{23}$$

An atomic oxygen scale height was adopted for the neutral atmosphere scale height $H_n \approx 30$ km. This equation (23) value of $Q_{\mathrm{esc,O}}$ is about 5–10% of the photochemical neutral O loss rate derived earlier but was largely based on a crude visual assessment of electron density profiles. A very large number of papers, both observational and modeling [cf. *Lundin et al*., 2013; *Brain et al*., 2015; *Ma et al*., 2015], and the large number of references in these papers have addressed the global ion escape issue with typical numbers being

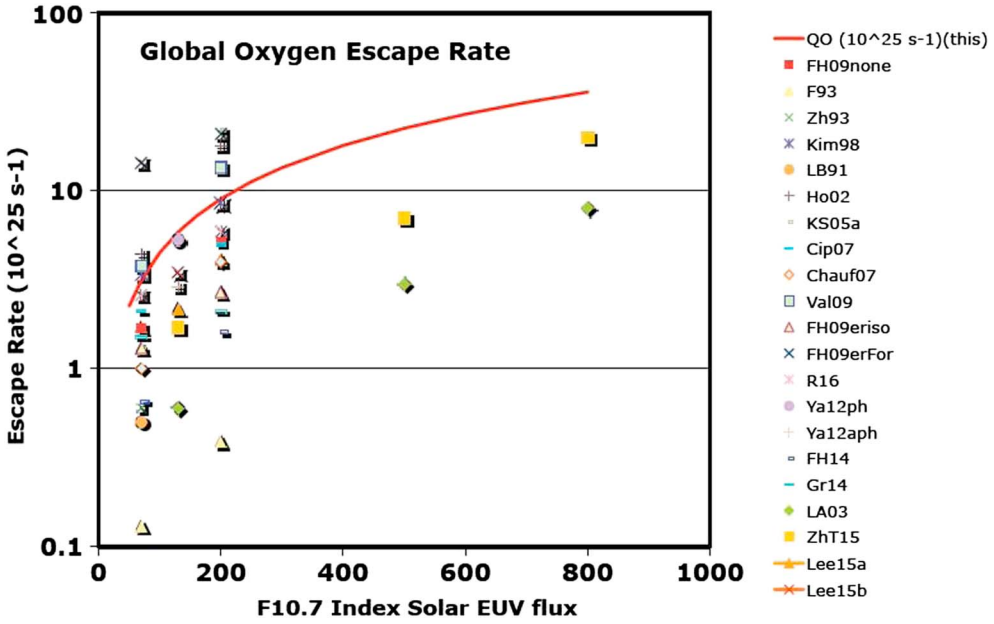

Figure 6. The relation between hot O escape flux and $F_{10.7}$ index of solar activity, as discussed in the text, is shown. The solid red line is the linear relation from the current paper (but on a log scale). Comparison values from a large number of models for different solar activity levels are shown. Table 3 provides the references for these models, as listed in the legend.

$Q_{esc,O} \approx 3\times10^{24}$–$3\times10^{25}\,s^{-1}$. The purpose of the current discussion was to tie the ion transport escape rate to a given solar activity level (e.g., MAVEN epoch) and to a critical neutral density so that $Q_{esc,O}$ can be extrapolated to other epochs more easily. This task will have to be revisited in the future so that the observational and modeling results can be viewed from this perspective.

The above analysis was relevant to draped magnetic field regions and not to crustal magnetic field regions. Regions of the ionosphere containing strong enough crustal magnetic fields should be shielded from direct solar wind effects, and the ion transport should be constrained to be mainly parallel to the magnetic field. All such ions produced along closed magnetic field lines should sooner or later flow down to lower altitudes and be photochemically processed (resulting in photochemical loss), even those ions created at high altitudes.

8. Implications for Past Mars Atmospheric Loss

Estimates of oxygen escape rates in the current epoch vary greatly in the literature so that it is not surprising that estimates of escape rates for the early Mars are even more uncertain. Figure 6 and Table 3 provide a comparison of global photochemical oxygen loss rates from a number of hot O models. *Fox and Hać* [2014] describe the cross sections used by several of the papers listed in Table 3. Table 4 in *Lee et al.* [2015a] also lists global oxygen escape rates for low and high solar activity from several sources. The simple linear loss rate from equation (19) as a function of the $F_{10.7}$ index of solar activity as suggested by equation (17) is shown as the solid line.

Zhang et al. [1993] estimated oxygen escape rates for ancient Mars and adopted the solar EUV irradiances versus age of the solar system suggested by *Zahnle and Walker* [1982]—for example, 5 times current irradiance for a solar system age of 1 Byr. The solar wind speed was also assumed to be higher in the past (2–3 times greater than current value of ≈350 km/s at an age of 1 Byr) [*Newkirk*, 1980]. *Zhang et al.* carried out two-stream hot O calculations and found photochemical O escape rates of $7\times10^{25}\,s^{-1}$, $4\times10^{26}\,s^{-1}$, and $10^{27}\,s^{-1}$ for solar EUV levels of 1 times, 3 times, and 6 times current values, respectively [also see *Ergun et al.*, 2016]. The *Zhang et al.* value for the current epoch is not too different from the estimate in the current paper (and some of the other estimates in the literature). The increase of O escape with increasing EUV level in the *Zhang et al.* study is somewhat greater than linear but less than quadratic, whereas in the current paper

Table 3. Models of Photochemical Oxygen Escape at Mars—Papers in Figure[a]

Symbol	Reference	Comments (See Actual Reference)
FH09none	*Fox and Hać* [2009]	noneroded ionosphere (superceded by *Fox and Hać* [2014]
F93	*Fox* [1993]	eroded ionosphere
Zh93	*Zhang et al.* [1993]	
Kim98	*Kim et al.* [1998]	as corrected by *Nagy et al.* [2001]
LB91	*Lammer and Bauer* [1991]	
Ho02	*Hodges* [2002]	
KS05a	*Krestyanikova and Shematovich* [2005]	as corrected by *Luhmann* [1997]
Cip07	*Cipriani et al.* [2007]	
Chauf07	*Chaufray et al.* [2007]	
Val09	*Valeille et al.* [2009a, 2009b]	
FH09eriso	*Fox and Hać* [2009]	eroded ionosphere; isotropic scattering
FH09erFor	*Fox and Hać* [2009]	eroded ionosphere; forward scattering
R16	*Rahmati* [2016]	also see *Rahmati et al.* [2014]
Ya12ph	*Yagi et al.* [2012]	Mars perihelion
Ya12aph	*Yagi et al.* [2012]	Mars aphelion
FH14	*Fox and Hać* [2014]	
Gr14	*Gröller et al.* [2014]	
LA03	*Lammer et al.* [2003]	
ZhT15	*Zhao and Tian* [2015]	
Lee15a	*Lee et al.* [2015a]	perihelion, moderate activity
Lee15b	*Lee et al.* [2015b]	autumn, three solar activities

[a]Solar minimum was given the value $F_{10.7} = 70$. Solar maximum was given the value $F_{10.7} = 200$. Moderate/unspecified solar activity was given the value $F_{10.7} = 130$. Values in the associated figure for references prior to 2010 were taken from *Fox and Hać* [2009].

we predict a simple linear relation. *Lammer et al.* [2003, 2008] estimated an O escape rate that is about 10 times greater than current values for a time 3.5 Ga ago.

More recently, *Zhao and Tian* [2015] revisited past epoch photochemical escape rates using one-dimensional Monte Carlo methods. The increase of escape rate with EUV flux was much less than that found by *Zhang et al.* [1993] or by *Lammer et al.* [2003] for EUV levels less than 10 times current values, and the photochemical escape rate actually decreased for EUV levels more than 10 times current levels. The decline in escape rate for very high EUV levels was attributed to changes in the underlying thermospheric composition, that is, more atomic species due to increased photodissociation. However, it seems to us that this decrease in photochemical loss might be compensated for by an increased ion transport and loss.

9. Conclusions

Current models of hot oxygen at Mars differ in their methods and in their results [*Lillis et al.*, 2015; cf. references in section 1] with photochemical oxygen escape rates varying from $10^{24}\,s^{-1}$ up to $10^{26}\,s^{-1}$ (Figure 6). The escape fluxes differ not so much because the methods (two-stream or Monte Carlo) are different but because the elastic oxygen cross sections used in the models differ, with current models mainly extrapolating from the theoretically calculated O-O cross section of *Kharchenko et al.* [2000]. All models show an increased escape rate for larger solar EUV fluxes, although there are major uncertainties in how to extrapolate these O loss rates back to early Mars conditions.

The current paper developed simple expressions for photochemical oxygen loss and for ion loss in order to make the dependencies on solar flux level and on cross sections more transparent. The issue of how atmospheric composition affects escape remains more problematic, but overall the expressions derived in this paper are probably robust with respect to changes in the details of the atmosphere and ionosphere.

In summary, the photochemical oxygen escape flux expression was found to be

$$F_{\mathrm{esc,\ O}} \approx 0.1\ I_{CO2}(1\ \mathrm{AU})/\sigma_{\mathrm{O\text{-}CO2}} \approx 1.4\times10^{8}(F10.7/200)\ \ \mathrm{cm}^{-2}\ \ \mathrm{s}^{-1}$$
$$\mathrm{Globally},\ \ Q_{\mathrm{esc,\ O}} \approx Q \approx 9\times10^{25}(F10.7/200)\ \ \mathrm{s}^{-1} \tag{24}$$

where I_{CO2} is the solar photoionization frequency for CO_2 at 1 AU and $\sigma_{\mathrm{O\text{-}CO2}}$ is the backscatter cross section for O collisions with CO_2. For solar maximum conditions equation (24) gives $F_{\mathrm{esc,O}} \approx 1.4\times10^{8}\,\mathrm{cm}^{-2}\,\mathrm{s}^{-1}$ and a

global O loss rate of $Q \approx 9 \times 10^{25}\,s^{-1}$. The escape flux should be roughly independent of solar zenith angle almost out to the terminator. The total ion loss rate discussed in section 7 is about 5–10% of the photochemical loss rate.

The details that went into estimating the production efficiency factor *f* (see section 5.1) or into how much of the elastic cross section is really backscattering or what the neutral composition effects really are will require detailed hot O photochemical models and ion loss models such as those found in the literature, but the current paper provides a simple context within which the numerical results can be examined and compared. Note that full hot O density profiles can only come from the more detailed models. Given the uncertainties in the elastic cross sections, the most important task in the near future for the hot O problem is to make model comparisons with MAVEN measurements of the hot O density and escape rates now being carried out by the Imaging Ultraviolet Spectrograph instrument [e.g., *Deighan et al*., 2015] and the measurements of pickup O^+ fluxes by the Solar Energetic Particle, Solar Wind Ion Analyzer, and Suprathermal and Thermal Ion Composition instruments [*Rahmati et al*., 2014, 2017]. These comparisons of models with MAVEN data will allow the determination of an empirical, or effective, elastic backscatter cross section as well as testing other assumptions in these models.

Acknowledgments
MAVEN data are available in the Planetary Data System. All data shown in the figures can be obtained from the corresponding author. This work was supported at the University of Kansas by NASA grant NNH10CC04C to the University of Colorado and by subcontract to the University of Kansas. S. Bougher was supported by a MAVEN/University of Colorado subcontract to the University of Michigan. The MAVEN project is supported by NASA through the Mars Exploration Program.

References

Benna, M., P. R. Mahaffy, J. M. Grebowsky, J. L. Fox, R. V. Yelle, and B. M. Jakosky (2015), First measurements of composition and dynamics of the Martian ionosphere by MAVEN's neutral gas and ion mass spectrometer, *Geophys. Res. Lett.*, *42*, 8958–8965, doi:10.1002/2015GL065146.

Bougher, S. W., D. Pawlowski, J. Bell, S. Nelli, T. McDunn, J. Murphy, M. Chizek, and A. Ridley (2015a), Mars Global Ionosphere Thermosphere Model (M-GITM): I. Solar cycle, seasonal, and diurnal variations of the upper atmosphere, *J. Geophys. Res. Planets*, *120*, 311–342, doi:10.1002/2014JE004715.

Bougher, S. W., et al. (2015b), Early MAVEN deep dip campaign reveals thermosphere and ionosphere variability, *Science*, *350*(6261), aad0459, doi:10.1126/science.aad0459.

Bougher, S. W., T. E. Cravens, J. Grebowsky, and J. Luhmann (2015c), The aeronomy of Mars: Characterization by MAVEN of the upper atmosphere reservoir that regulates volatile escape, *Space Sci. Rev.*, *195*, 423, doi:10.1007/s11214-014-0053-7.

Brain, D. A., et al. (2015), The spatial distribution of planetary ion fluxes near Mars observed by MAVEN, *Geophys. Res. Lett.*, *42*, 9142–9148, doi:10.1002/2015GL065293.

Chaufray, J. Y., R. Modolo, F. Leblanc, G. Chanteur, R. E. Johnson, and J. G. Luhmann (2007), Mars solar wind interaction: Formation of the Martian corona and atmospheric loss to space, *J. Geophys. Res.*, *112*, E09009, doi:10.1029/2007JE002915.

Chen, R. H., T. E. Cravens, and A. F. Nagy (1978), The Martian ionosphere in light of the Viking observations, *J. Geophys. Res.*, *83*, 3871–3876, doi:10.1029/JA083iA08p03871.

Cipriani, F., F. LeBlanc, and J. J. Berthelier (2007), Martian corona: Nonthermal sources of hot heavy species, *J. Geophys. Res.*, *112*, E09009, doi:10.1029/2007JE002915.

Cravens, T. E., J. U. Kozyra, A. F. Nagy, T. I. Gombosi, and M. Kurtz (1987), Electron impact ionization in the vicinity of comets, *J. Geophys. Res.*, *92*, 7341–7353, doi:10.1029/JA092iA07p07341.

Cravens, T. E., et al. (2010), Dynamical and magnetic field time constants for Titan's ionosphere—Empirical estimates and comparisons with Venus, *J. Geophys. Res.*, *115*, A08319, doi:10.1029/2009JA015050.

Deighan, J., et al. (2015), MAVEN IUVS observation of the hot oxygen corona at Mars, *Geophys. Res. Lett.*, *42*, 9009–9014, doi:10.1002/2015GL065487.

Dong, C., S. W. Bougher, Y. Ma, G. Toth, A. F. Nagy, and D. Najib (2014), Solar wind interaction with Mars upper atmosphere: Results from the one-way coupling between the multi-fluid MHD model and the MTGCM model, *Geophys. Res. Lett.*, *41*, 2708–2715, doi:10.1002/2014GL059515.

Ergun, R. E., L. Andersson, W. K. Peterson, D. Brain, G. T. Delory, D. L. Mitchell, R. P. Lin, and A. W. Yau (2006), Role of plasma waves in Mars' atmospheric loss, *Geophys. Res. Lett.*, *33*, L14103, doi:10.1029/2006GL025785.

Ergun, R. E., M. W. Morooka, L. A. Andersson, C. M. Fowler, G. T. Delory, D. J. Andrews, A. I. Eriksson, T. McEnulty, and B. M. Jakosky (2015), Dayside electron temperature and density profiles at Mars: First results from the MAVEN Langmuir probe and waves instrument, *Geophys. Res. Lett.*, *42*, 8846–8853, doi:10.1002/2015GL065280.

Ergun, R. E., et al. (2016), Enhanced O_2^+ loss at Mars due to an ambipolar electric field from electron heating, *J. Geophys. Res. Space Physics*, *121*, 4668–4678, doi:10.1002/2016JA022349.

Fox, J. L. (1993), The production and escape of nitrogen atoms on Mars, *J. Geophys. Res.*, *98*, 3297–3310, doi:10.1029/92JE02289.

Fox, J. L. (1997), Upper limits to the outflow of ions at Mars: Implications for atmospheric evolution, *Geophys. Res. Lett.*, *24*, 2901–2904, doi:10.1029/97GL52842.

Fox, J. L. (2009), Morphology of the dayside ionosphere of Mars: Implication for ion outflows, *J. Geophys. Res.*, *114*, E12005, doi:10.1029/2009JE003432.

Fox, J. L., and A. B. Hać (2009), Photochemical escape of oxygen from Mars: A comparison of the exobase approximation to a Monte Carlo method, *Icarus*, *204*, 527–544, doi:10.1016/j.icarus.2009.07.005.

Fox, J. L., and A. B. Hać (2014), The escape of O from Mars: Sensitivity to the elastic cross sections, *Icarus*, *228*, 375–385, doi:10.1016/j.icarus.2013.10.014.

Fox, J. L., M. Benna, P. R. Mahaffy, and B. M. Jakosky (2015), Water and water ions in the Martian thermosphere/ionosphere, *Geophys. Res. Lett.*, *42*, 8977–8985, doi:10.1002/2015GL065465.

Fränz, M., E. Dubinin, E. Nielsen, J. Woch, S. Barabash, R. Lundin, and A. Fedorov (2010), Transterminator ion flow in the Martian ionosphere, *Planet. Space Sci.*, *58*, 1442–1454, doi:10.1016/j.pss.2010.06.009.

Gröller, H., H. Lichtenegger, H. Lammer, and V. I. Shematovich (2014), Hot oxygen and carbon escape from the Martian atmosphere, *Planet. Space Sci.*, *98*, 93–105, doi:10.1016/j.pss.2014.01.007.

Hanson, W. B., and G. P. Mantas (1988), Viking electron temperature measurements: Evidence of a magnetic field in the Martian ionosphere, *J. Geophys. Res.*, *93*, 7538–7544, doi:10.1029/JA093iA07p07538.
Hanson, W. B., S. Sanatani, and D. R. Zuccaro (1977), The Martian ionosphere as observed by the Viking retarding potential analyzers, *J. Geophys. Res.*, *82*, 4351–4363, doi:10.1029/JS082i028p04351.
Hodges, R. R. (2000), Distributions of hot oxygen for Venus and Mars, *J. Geophys. Res.*, *105*, 6971–6981, doi:10.1029/1999JE001138.
Hodges, R. R. (2002), The rate of loss of water from Mars, *Geophys. Res. Lett.*, *29*(3), 1038, doi:10.1029/2001GL013853.
Johnson, R. E., and J. G. Luhmann (1998), Sputter contribution to the atmospheric corona on Mars, *J. Geophys. Res.*, *103*, 3649–3653, doi:10.1029/97JE03266.
Kharchenko, V., A. Dalgarno, B. Zygelman, and J. H. Yee (2000), Energy transfer in collisions of oxygen atoms in the terrestrial atmosphere, *J. Geophys. Res.*, *105*(24), 24,899–24,906, doi:10.1029/2000JA000085.
Kim, J., A. F. Nagy, J. L. Fox, and T. E. Cravens (1998), Solar cycle variability of hot oxygen atoms at Mars, *J. Geophys. Res.*, *103*, 29,339–29,342, doi:10.1029/98JA02727.
Krestyanikova, M. A., and V. I. Shematovich (2005), Stochastic models of hot planetary and satellite coronas: A photochemical source of hot oxygen in the upper atmosphere of Mars, *Sol. Syst. Res.*, *39*, 22–32, doi:10.1007/s11208-005-0002-9.
Lammer, H., and S. J. Bauer (1991), Nonthermal atmospheric escape from Mars and Titan, *J. Geophys. Res.*, *96*, 1819–1825, doi:10.1029/90JA01676.
Lammer, H., H. I. M. Lichtenegger, C. Kolb, I. Ribas, E. F. Guinan, R. Abart, and S. J. Bauer (2003), Loss of water from Mars: Implications for the oxidation of the soil, *Icarus*, *165*, 9–25, doi:10.1016/S0019-1035(03)00170-2.
Lammer, H., J. F. Kasting, E. Chassefiere, R. E. Johnson, Y. N. Kulikov, and F. Tian (2008), Atmospheric escape and evolution of terrestrial planets and satellites, *Space Sci. Rev.*, *139*(1), 399–436, doi:10.1007/978-0-387-87825-6_11.
Lee, Y., M. R. Combi, V. Tenishev, S. W. Bougher, and R. J. Lillis (2015a), Hot oxygen corona at Mars and the photochemical escape of oxygen: Improved description of the thermosphere, ionosphere and exosphere, *J. Geophys. Res. Planets*, *120*, 1880–1892, doi:10.1002/2015JE004890.
Lee, Y., M. R. Combi, V. Tenishev, S. W. Bougher, J. Deighan, N. M. Schneider, W. E. McClintock, and B. M. Jakosky (2015b), A comparison of 3-D model predictions of Mars' oxygen corona with early MAVEN IUVS observations, *Geophys. Res. Lett.*, *42*, 9015–9022, doi:10.1002/2015GL065291.
Lillis, R. J., et al. (2015), Characterizing atmospheric escape from Mars today and through time, with MAVEN, *Space Sci. Rev.*, *195*, 357–422, doi:10.1007/s11214-015-0165-8.
Luhmann, J. G. (1997), Correction to "The ancient oxygen exosphere of Mars: Implications for atmosphere evolution" by Zhang et al., *J. Geophys. Res. 102*, 1637, doi:10.1029/96JE03440.
Luhmann, J. G., and T. E. Cravens (1991), Magnetic fields in the ionosphere of Venus, *Space Sci. Rev.*, *55*, 201–274, doi:10.1007/BF00177138.
Lundin, R., S. Barabash, M. Holmstrom, H. Nilsson, Y. Futaana, R. Ramstad, M. Yamauchi, E. Dubinin, and M. Fraenz (2013), Solar cycle effects on the ion escape from Mars, *Geophys. Res. Lett.*, *40*, 6028–6032, doi:10.1002/2013GL058154.
Ma, Y. J., et al. (2015), MHD model results of solar wind interaction with Mars and comparison with MAVEN plasma observations, *Geophys. Res. Lett.*, *42*, 9113–9120, doi:10.1002/2015GL065218.
Mahaffy, P. R., et al. (2015), The neutral gas and ion mass spectrometer on the Mars atmosphere and volatile evolution mission, *Space Sci. Rev.*, *195*, 49–73, doi:10.1007/s11214-014-0091-1.
Matta, M., P. Withers, and M. Mendillo (2013), The composition of Mars' topside ionosphere: Effects of hydrogen, *J. Geophys. Res. Space Physics*, *2681*, –2693, doi:10.1002/jgra.50104.
Matta, M., M. Galand, L. Moore, M. Mendillo, and P. Withers (2014), Numerical simulations of ion and electron temperatures in the ionosphere of Mars: Multiple ions and diurnal variations, *Icarus*, *227*, 78–88, doi:10.1016/j.icarus.2013.09.006.
McElroy, M. B. (1972), Mars: An evolving atmosphere, *Science*, *175*, 443–445, doi:10.1126/science.175.4020.443.
Nagy, A. F., and T. E. Cravens (1988), Hot oxygen atoms in the upper atmospheres of Venus and Mars, *Geophys. Res. Lett.*, *15*(5), 433–435, doi:10.1029/GL015i005p00433.
Nagy, A. F., T. E. Cravens, J. H. Yee, and A. I. Stewart (1981), Hot oxygen atoms in the upper atmosphere of Venus, *Geophys. Res. Lett.*, *8*, 629–632, doi:10.1029/GL008i006p00629.
Nagy, A. F., J. Kim, and T. E. Cravens (1990), Hot hydrogen and oxygen atoms in the upper atmospheres of Venus and Mars, *Ann. Geophys.*, *8*, 251.
Nagy, A. F., M. W. Liemohn, J. L. Fox, and J. Kim (2001), Hot carbon densities in the exosphere of Mars, *Geophys. Res. Lett.*, *82*, 4341–4349.
Newkirk, G., Jr. (1980), Solar variability on time scales of 10^5 years to $10^{9.6}$ years, in *The Ancient Sun*, *Geochim. Cosmochim. Acta Suppl.*, vol. 13, edited by R. O. Pepin, J. A. Eddy, and R. B. Merrill, pp. 293, Pergamon Press.
Petrignani, A., F. Hellberg, R. D. Thomas, M. Larsson, P. C. Cosby, and W. J. van der Zande (2005), Electron energy-dependent product state distributions in the dissociative recombination of O_2^+, *J. Chem. Phys.*, *122*(23), 234–311, doi:10.1063/1.1937388.
Peverall, R., et al. (2001), Dissociative recombination and excitation of O_2^+: Cross sections, product yields and implications for studies of ionospheric airglows, *J. Chem. Phys.*, *114*, 6679–6689, doi:10.1063/1.1349079.
Rahmati, A. (2016), Oxygen exosphere of Mars: Evidence from pickup ions measured by MAVEN PhD thesis, Univ. of Kansas.
Rahmati, A., T. E. Cravens, A. F. Nagy, J. L. Fox, S. W. Bougher, R. J. Lillis, S. A. Ledvina, D. E. Larson, P. Dunn, and J. A. Croxell (2014), Pickup ion measurements by MAVEN: A diagnostic of photochemical oxygen escape from Mars, *Geophys. Res. Lett.*, *41*, 4812–4818, doi:10.1002/2014GL060289.
Rahmati, A., D. E. Larson, T. E. Cravens, R. J. Lillis, P. A. Dunn, J. S. Halekas, J. E. Connerney, F. G. Eparvier, E. M. B. Thiemann, and B. M. Jakosky (2015), MAVEN insights into oxygen pickup ions at Mars, *Geophys. Res. Lett.*, *42*, 8870–8876, doi:10.1002/2015GL065262.
Rahmati, A., et al. (2017), MAVEN measured oxygen and hydrogen pickup ions: Probing the Martian exosphere and neutral escape, *J. Geophys. Res. Space Physics*, *122*, doi:10.1002/2016JA023371, in press.
Sakai, S., A. Rahmati, D. L. Mitchell, T. E. Cravens, S. W. Bougher, C. Mazelle, W. K. Peterson, F. G. Eparvier, J. M. Fontenla, and B. M. Jakosky (2015), Model insights into energetic photoelectrons measured at Mars by MAVEN, *Geophys. Res. Lett.*, *42*, 8894–8900, doi:10.1002/2015GL065169.
Sakai, S., et al. (2016), Electron energetics in the Martian dayside ionosphere: Model comparisons with MAVEN data, *J. Geophys. Res. Space Physics*, *121*, 7049–7066, doi:10.1002/2016JA022782.
Schunk, R. W., and A. F. Nagy (2009), *Ionospheres: Physics, Plasma Physics, and Chemistry*, 2nd ed., Cambridge Univ. Press, Cambridge, U. K.
Valeille, A., V. Tenishev, M. Combi, S. Bougher, and A. Nagy (2009a), 3D study of Mars upper-thermosphere/ionosphere and hot corona: (1) General description and results at equinox for solar minimum conditions, *J. Geophys. Res.*, *114*, E11005, doi:10.1029/2009JE003388.
Valeille, A., V. Tenishev, M. Combi, S. Bougher, and A. Nagy (2009b), 3D study of Mars upper-thermosphere/ionosphere and hot corona: (2) Solar cycle, seasonal variations, and evolution over history, *J. Geophys. Res.*, *114*, E11006, doi:10.1029/2009JE003389.

Valeille, A., M. R. Combi, V. Tenishev, S. W. Bougher, and A. F. Nagy (2010a), A study of suprathermal oxygen atoms in Mars upper thermosphere and exosphere over the range of limiting conditions, *Icarus*, *206*, 18–27, doi:10.1016/j.icarus.2008.08.018.

Valeille, A., S. W. Bougher, V. Tenishev, M. R. Combi, and A. F. Nagy (2010b), Water loss and evolution of the upper atmosphere and exosphere over Martian history, *Icarus*, *206*, 28–39, doi:10.1016/j.icarus.2009.04.036.

Vogt, M. F., et al. (2015), Ionopause-like density gradients in the Martian ionosphere: A first look with MAVEN, *Geophys. Res. Lett.*, *42*, 8885–8893, doi:10.1002/2015GL065269.

Withers, P., et al. (2015), Comparison of model predictions for the composition of the ionosphere of Mars to MAVEN NGIMS data, *Geophys. Res. Lett.*, *42*, 8966–8976, doi:10.1002/2015GL065205.

Yagi, M., F. Leblanc, J. Y. Chaufray, F. Gonzalez-Galindo, S. Hess, and R. Modolo (2012), Mars exospheric thermal and non-thermal components: Seasonal and local variations, *Icarus*, *221*, 682–693, doi:10.1016/j.icarus.2012.07.022.

Yee, J. H., J. W. Meriwether Jr., and P. B. Hays (1980), Detection of a corona of fast atoms during solar maximum, *J. Geophys. Res.*, *85*, 3396–3400, doi:10.1029/JA085iA07p03396.

Zahnle, K., and A. Walker (1982), The evolution of solar ultraviolet luminosity, *Rev. Geophys.*, *20*, 280–292, doi:10.1029/RG020i002p00280.

Zhang, M. H. G., J. G. Luhmann, S. W. Bougher, and A. F. Nagy (1993), The ancient oxygen atmosphere of Mars: Implications for atmosphere evolution, *J. Geophys. Res.*, *98*, 10,915–10,923, doi:10.1029/93JE00231.

Zhao, J., and F. Tian (2015), Photochemical escape of oxygen from early Mars, *Icarus*, *250*, 477–481, doi:10.1016/j.icarus.2014.12.032.